

Preserved travel-time smoothing in orthorhombic media

Shibo Xu* and Alexey Stovas

Department of Petroleum Engineering and Applied Geophysics, Norwegian University of Science and Technology, S.P. Andersens veg 15a, NO-7491, Trondheim, Norway

Received March 2016, revision accepted October 2016

ABSTRACT

Certain degree of smoothness of velocity models is required for most ray-based migration and tomography. Applying conventional smoothing in model parameters results in offset-dependent travel-time errors for reflected events, which can be large even for small contrasts in model parameters between the layers. This causes the shift in both the depth and residual moveout of the migrated images. To overcome this problem in transversely isotropic medium with a vertical symmetry axis, the preserved travel-time smoothing method was proposed earlier. We extend this method for orthorhombic media with and without azimuthal variation between the layers. We illustrate this method for a single interface between two orthorhombic layers and show that the smoothing-driven errors in travel time are very small for practical application.

Key words: Velocity model, Smoothing, Orthorhombic medium.

INTRODUCTION

Velocity models for prestack depth migration are commonly built by layer stripping with velocity discontinuities across the horizons. The ray tracing (Červený 2001) used in Kirchhoff or beam migration requires certain smoothness of the depth velocity model. The current industrial practice for smoothing is to perform a bell-shaped filter (Gonzalez and Woods 2008) to the step of model parameters. The drawback of conventional smoothing is that the migrated events will shift to a higher velocity layer at the discontinuities compared with results from the unsmoothed model. The shift is offset dependent, and the errors in depth and the residual moveout for the migrated images are induced by the smoothing process, which will cause errors in velocity analysis. Several approaches are proposed for this problem like adding the horizons in the ray-tracing process (Vinje *et al.* 1996) and combining the unsmoothed and smoothed models (Baina, Zamboni and Lambaré 2006). The preserved travel-time smoothing (PTS) method (Vinje, Stovas and Reynaud 2012) is proposed to solve this problem based on the kinematically equivalent media (Stovas 2008) and the travel-time filter. It is designed to smooth the depth

models accompanied by preserving the travel-time parameters at the velocity discontinuities.

The orthorhombic (ORT) medium is introduced by Schoenberg and Helbig (1997) to describe the fractured earth and has become a new standard to define model parameters to cover the azimuthal dependence of the travel-time surface. Tsvankin (1997, 2012) defines the elastic ORT model with nine parameters that can be reduced to six parameters in an acoustic approximation (Alkhalifah 2003). These parameters are vertical velocity V_0 , two local normal moveout (NMO) velocities defined in vertical symmetry planes, and three local anelliptic parameters. The anelliptic parameters can be defined in all symmetry planes (Grechka and Tsvankin 1999a) or can be defined in terms of azimuthally dependent anellipticity (Stovas 2015). In addition to this, we might have one extra parameter responsible for azimuthal orientation of the symmetry planes.

In this paper, we extend the PTS method to an ORT model based on the azimuthal dependence of kinematic properties defined for an acoustic ORT medium (Stovas 2015) to preserve the travel-time parameters for smoothed ORT model. In case of azimuthal variations in the symmetry axis between the layers, the least squares approximation is adopted to estimate the effective anellipticity parameters from this layered

*E-mail: shibo.xu@ntnu.no

medium to preserve the complexity of the model when doing smoothing (ORT both input and output). The travel-time parameters are preserved for the azimuthally dependent ORT model, and the resulting error in travel time is sufficiently small from the numerical examples. In our paper, we focus on defining the composite parameters only and use very simple Gaussian filter instead of the complicated smoothing operator as proposed in Vinje *et al.* (2012).

VELOCITY MOMENTS AND COMPOSITE PARAMETERS FOR A TRANSVERSELY ISOTROPIC MODEL WITH A VERTICAL SYMMETRY AXIS

In order to preserve travel time when smoothing the velocity model, Vinje *et al.* (2012) define the depth-dependent composite parameterisation of a transversely isotropic model with a vertical symmetry axis (VTI) medium under the acoustic approximation (Alkhalifah 1998) represented by kinematic parameters (Stovas 2008)

$$\begin{aligned} m_1(\xi) &= \frac{1}{V_0(\xi)}, \\ m_2(\xi) &= \frac{V_{nmo}^2(\xi)}{V_0(\xi)}, \\ m_3(\xi) &= \frac{V_{nmo}^4(\xi)(1 + 8\eta(\xi))}{V_0(\xi)}, \end{aligned} \quad (1)$$

where m_1 , m_2 , and m_3 are the unsmoothed composite parameters; and V_0 is the vertical P-wave velocity; and V_{nmo} is the normal moveout velocity defined by $V_{nmo} = V_0\sqrt{1 + 2\delta}$, $\eta = (\varepsilon - \delta)/(1 + 2\delta)$, where δ and ε are the anisotropy parameters (Thomsen 1986).

Composite parameters m_1 , m_2 , and m_3 are smoothed by Gaussian filter so that the velocity moments are preserved at the velocity discontinuities. It means that the integral for

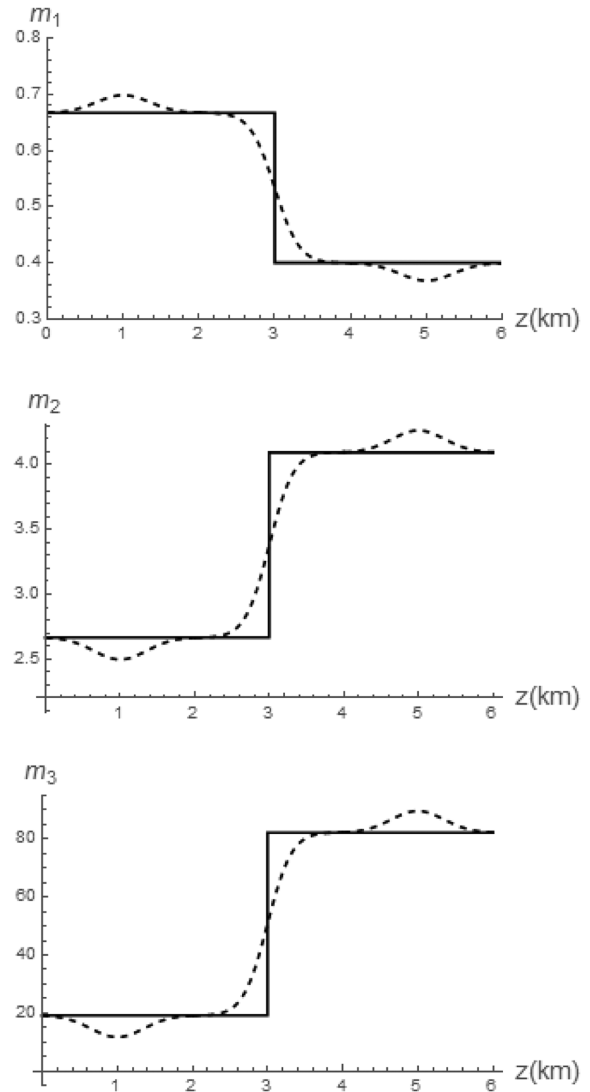


Figure 2 Composite parameters (top) m_1 , (middle) m_2 , and (bottom) m_3 before and after smoothing for the VTI model. The unsmoothed and smoothed parameters are shown by solid and dashed lines, respectively.

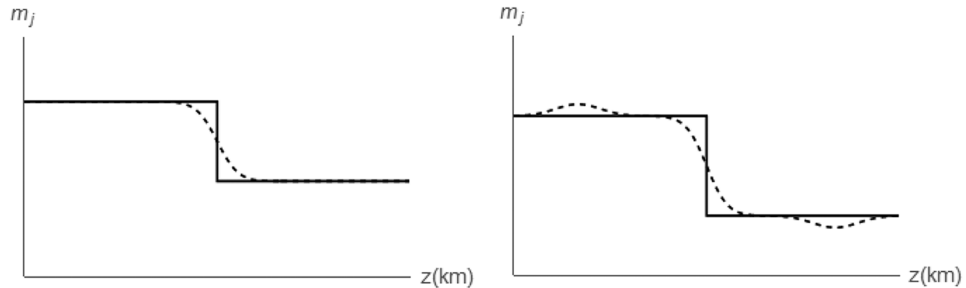


Figure 1 (Left) The unsmoothed and smoothed composite parameters. (Right) The same composite parameter with compensation functions. The unsmoothed and smoothed parameters are shown by solid and dashed lines, respectively.

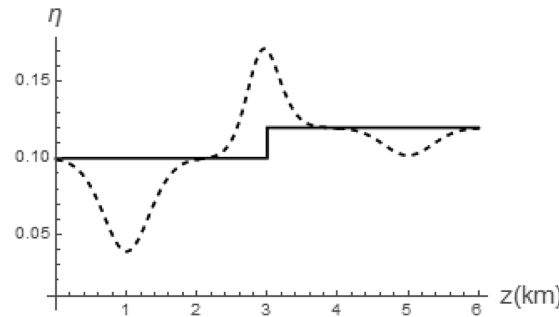
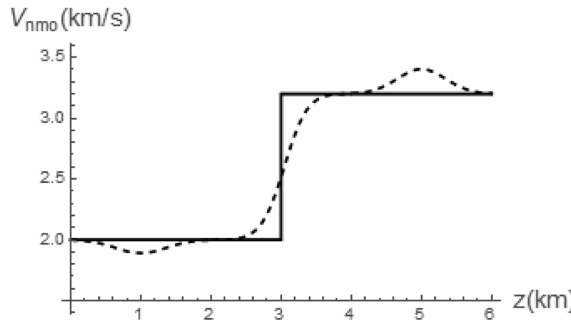
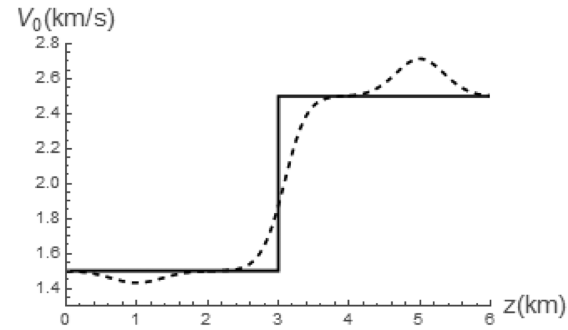


Figure 3 Model parameters (top) V_0 , (middle) V_{nmo} , and (bottom) η before and after smoothing for the VTI model. The unsmoothed and smoothed parameters are shown by solid and dashed lines, respectively.

composite parameter m_j (before and after smoothing) remains the same

$$\int_0^z m_j(\xi) d\xi = \int_0^z \tilde{m}_j(\xi) d\xi, \quad j = 1, 2, 3. \quad (2)$$

The model is studied in 1D (vertical direction); therefore, smoothing for the composite parameters is also computed in 1D, consequently.

The smoothed composite parameter \tilde{m}_j can be obtained by using a conventional Gaussian filter

$$\tilde{m}_j(z) = \frac{\int_{z-\Delta z/2}^{z+\Delta z/2} w(\xi) m_j(\xi) d\xi}{\int_{z-\Delta z/2}^{z+\Delta z/2} w(\xi) d\xi}, \quad (3)$$

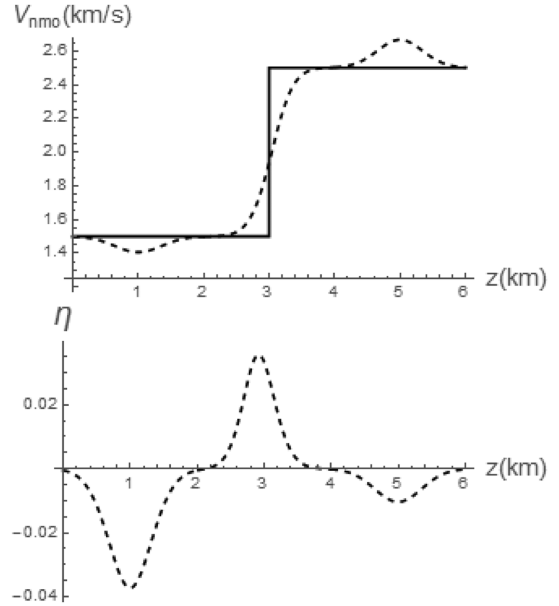


Figure 4 The kinematic parameters (top) V_{nmo} and (bottom) η computed for the ISO model.

where \tilde{m}_j and m_j are smoothed and unsmoothed composite parameters, respectively, and w is the Gaussian function and Δz is the length of the filter. Vinje *et al.* (2012) designed the special filter used for smoothing, but in this paper, we use the simple Gaussian filter for simplicity.

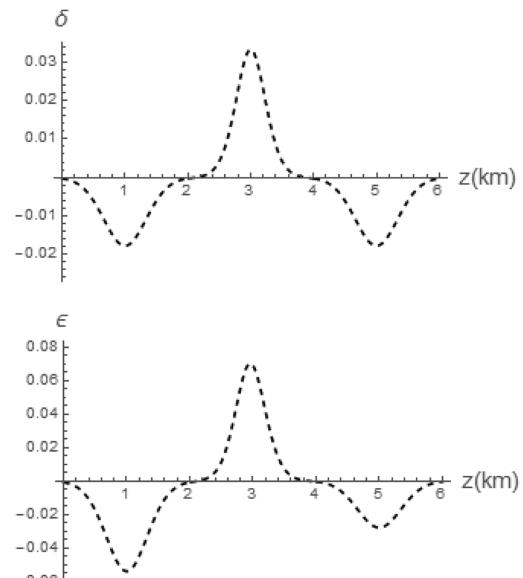


Figure 5 The smoothing-induced anisotropy parameters (top) δ and (bottom) ϵ computed for the ISO model.

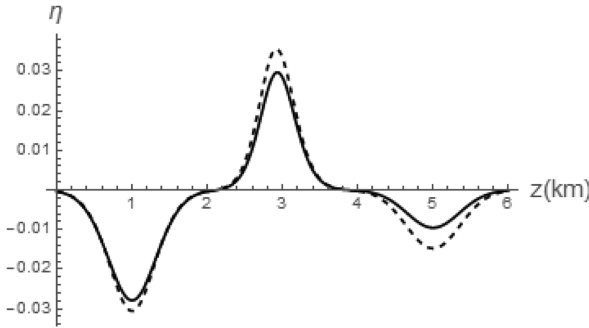


Figure 6 The induced anellipticity from the (solid line) EI and (dashed line) ISO models.

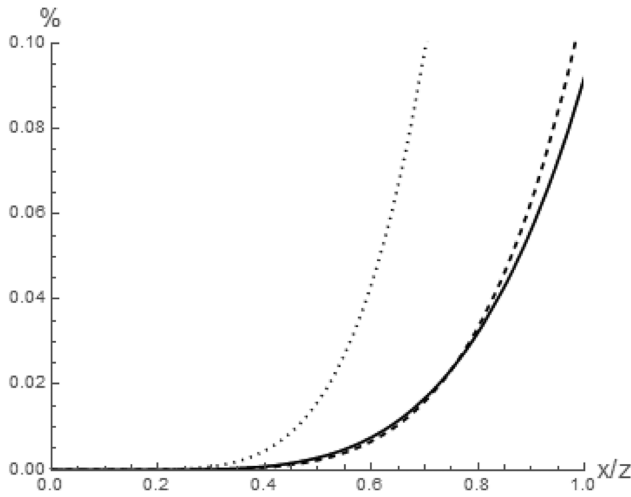


Figure 7 The travel-time error between two models, i.e., smoothed and unsmoothed, for the VTI, EI, and ISO cases shown by solid, dashed, and dotted lines, respectively.

The smoothed composite parameter \tilde{m}_j is shown in Fig. 1 (left). In order to preserve the travel-time parameters, compensation function needs to be added before and after the step (Fig. 1, right). Smoothed composite parameters \tilde{m}_1 , \tilde{m}_2 , and \tilde{m}_3 can be converted into the model parameters by the following equation (Vinje *et al.* 2012):

$$\begin{aligned}\tilde{V}_0(\xi) &= \frac{1}{\tilde{m}_1(\xi)}, \\ \tilde{V}_{nmo}(\xi) &= \sqrt{\frac{\tilde{m}_2(\xi)}{\tilde{m}_1(\xi)}}, \\ \tilde{\eta}(\xi) &= \frac{1}{8} \left(\frac{\tilde{m}_3(\xi)\tilde{m}_1(\xi)}{\tilde{m}_2^2(\xi)} - 1 \right).\end{aligned}\quad (4)$$

To illustrate the smoothing procedure and the accuracy of the method, we select a two-layer VTI model. The

parameters of the upper layer are $V_0 = 1.5$ km/s, $V_{nmo} = 2$ km/s, and $\eta = 0.1$; the parameters of the lower layer are $V_0 = 2.5$ km/s, $V_{nmo} = 3.2$ km/s, and $\eta = 0.12$; and the thickness for both layers is 3 km. Unsmoothed and smoothed composite parameters m_j ($j = 1, 2, 3$) computed for the model specified above are shown in Fig. 2. One can see that the smoothing operator in equation (3) performs very similarly for all composite parameters.

The corresponding smoothed model parameters computed in equation (4) are shown in Fig. 3. From these plots, one can see that the shape of the smoothed anellipticity parameter η is very different from other kinematic parameters at the interface.

If the unsmoothed velocity model is isotropic ($\delta = \varepsilon = 0$), preserved travel-time smoothing (PTS) results in the smoothing-induced anisotropy illustrated in Fig. 4. The behaviour of the smoothed V_{nmo} is similar to the behaviour of the smoothed V_0 (Fig. 3). However, the smoothing-induced anellipticity parameter is different from the one obtained for the VTI model. We can decompose kinematic parameters shown in Fig. 4 into anisotropic parameters δ and ε (Fig. 5). The smoothed anisotropic parameters δ and ε have similar shape. The induced anellipticity from the elliptic isotropic (EI) case and that from the isotropic (ISO) case are shown in Fig. 6. From this plot, one can see that the induced anellipticity from the ISO model is larger than the one obtained from the EI model.

In order to illustrate the accuracy of the proposed method, we compute the depth-dependent offset-travel time by the integrals (Fomel and Stovas 2010)

$$\begin{aligned}X(p) &= \int_0^z \frac{p V_{NMO}^2(\xi)}{V_0(\xi)(1 - 2\eta(\xi)p^2 V_{NMO}^2(\xi))^{3/2} \sqrt{1 - (1 + 2\eta(\xi))p^2 V_{NMO}^2(\xi)}} d\xi, \\ T(p) &= \int_0^z \frac{(1 - 2\eta(\xi)p^2 V_{NMO}^2(\xi))^2 + 2\eta(\xi)p^4 V_{NMO}^4(\xi)}{V_0(\xi)(1 - 2\eta(\xi)p^2 V_{NMO}^2(\xi))^{3/2} \sqrt{1 - (1 + 2\eta(\xi))p^2 V_{NMO}^2(\xi)}} d\xi,\end{aligned}\quad (5)$$

where $X(p)$ and $T(p)$ are the parametric offset and travel time represented by horizontal slowness p . The relative travel-time error between unsmoothed and smoothed VTI, EI, and ISO models with parameters mentioned above is shown in Fig. 7. From the plot, one can see that the travel-time error increases with offset, and the error is very small even for large offset. Notice that the PTS method applied for the VTI and EI models results in smaller travel-time error compared with the ISO model.

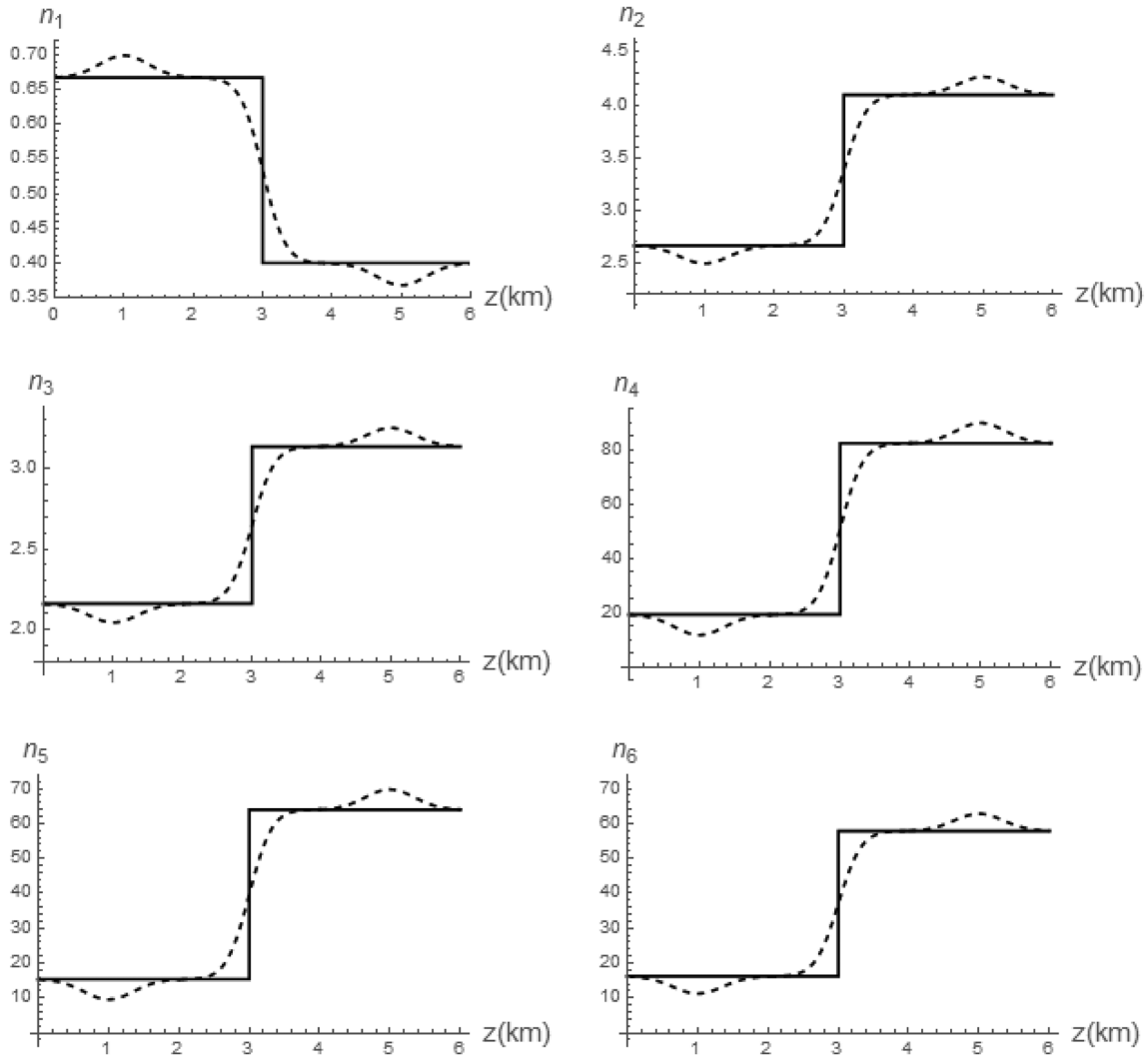


Figure 8 The composite parameters before and after smoothing for the ORT model. The unsmoothed and smoothed parameters are shown by solid and dashed lines, respectively.

PRESERVED TRAVEL-TIME SMOOTHING IN ORTHORHOMBIC MEDIA WITHOUT AZIMUTH VARIATION BETWEEN THE LAYERS

The kinematic properties in the orthorhombic (ORT) model without azimuth variation can be defined following Stovas (2015). The limited series for vertical slowness in the ORT medium is given by

$$\begin{aligned} q(p_x, p_y) = & \frac{1}{V_0} - \frac{p_x^2 V_{nmo1}^2}{2V_0} - \frac{p_y^2 V_{nmo2}^2}{2V_0} - \frac{(1+8\eta_1)p_x^4 V_{nmo1}^4}{8V_0} \\ & - \frac{(1+8\eta_2)p_y^4 V_{nmo2}^4}{8V_0} - \frac{(1+4\eta_{xy})p_x^2 p_y^2 V_{nmo1}^2 V_{nmo2}^2}{4V_0} + \dots, \end{aligned} \quad (6)$$

where q , p_x , and p_y denote the vertical and two horizontal projections of the slowness vector. The ORT medium parameters are vertical P-wave velocity V_0 and normal moveout (NMO) velocities V_{nmo1} and V_{nmo2} , which are defined in the $[x, z]$ and $[y, z]$ symmetry planes, respectively. The cross-term parameter η_{xy} is defined in Stovas (2015) as follows:

$$\eta_{xy} = \sqrt{\frac{(1+2\eta_1)(1+2\eta_2)}{1+2\eta_3}} - 1, \quad (7)$$

where η_1 , η_2 , and η_3 are the anellipticity parameters defined in symmetry planes $[x, z]$, $[y, z]$, and $[x, y]$, respectively.

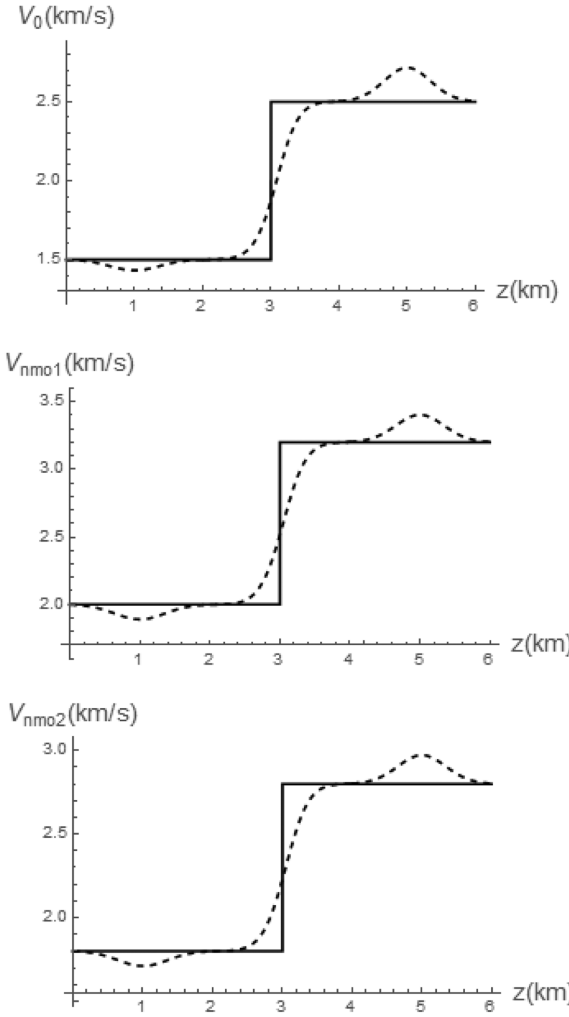


Figure 9 The model parameters (top) V_0 , (middle) V_{nmo1} , and (bottom) V_{nmo2} before and after smoothing for the ORT model. The unsmoothed and smoothed parameters are shown by solid and dashed lines, respectively.

For the ORT model with no azimuthal variation between the layers, we define that the depth-dependent composite parameters n_j ($j = 1, \dots, 6$) are based on series coefficients in equation (6)

$$\begin{aligned} n_1(\xi) &= \frac{1}{V_0(\xi)}, n_2(\xi) = \frac{V_{nmo1}^2(\xi)}{V_0(\xi)}, \\ n_3(\xi) &= \frac{V_{nmo2}^2(\xi)}{V_0(\xi)}, n_4(\xi) = \frac{V_{nmo1}^4(\xi)(1 + 8\eta_1(\xi))}{V_0(\xi)}, \\ n_5(\xi) &= \frac{V_{nmo2}^4(\xi)(1 + 8\eta_2(\xi))}{V_0(\xi)}, n_6(\xi) \\ &= \frac{V_{nmo1}^2(\xi)V_{nmo2}^2(\xi)(1 + 4\eta_{xy}(\xi))}{V_0(\xi)}. \end{aligned} \quad (8)$$

Three parameters in equation (8) are low order (two coefficients related to slowness squared and one constant term), whereas three others are high order (related to slowness to power four).

The first five composite parameters in equation (8) are similar to the ones defined for a VTI model, and only parameter n_6 is different. To illustrate the smoothing, we define a two-layer ORT model. The parameters for the upper layer are $V_0 = 1.5 \text{ km/s}$, $V_{nmo1} = 2 \text{ km/s}$, $V_{nmo2} = 1.8 \text{ km/s}$, $\eta_1 = 0.1$, $\eta_2 = 0.15$, and $\eta_{xy} = 0.22$, and the parameters for the lower layer are $V_0 = 2.5 \text{ km/s}$, $V_{nmo1} = 3.2 \text{ km/s}$, $V_{nmo2} = 2.8 \text{ km/s}$, $\eta_1 = 0.12$, $\eta_2 = 0.2$, and $\eta_{xy} = 0.2$. The thickness for both layers is 3 km. We show the smoothed composite parameters from equation (8) in Fig. 8. From these plots, we can see that smoothing curves for composite parameters are very similar with the ones obtained in the VTI case.

We convert the smoothed composite parameters into the model parameters by

$$\begin{aligned} \tilde{V}_0(\xi) &= \frac{1}{\tilde{n}_1(\xi)}, \tilde{V}_{nmo1}(\xi) = \sqrt{\frac{\tilde{n}_2(\xi)}{\tilde{n}_1(\xi)}}, \tilde{V}_{nmo2}(\xi) = \sqrt{\frac{\tilde{n}_3(\xi)}{\tilde{n}_1(\xi)}}, \\ \tilde{\eta}_1(\xi) &= \frac{\tilde{n}_4(\xi)\tilde{n}_1(\xi) - \tilde{n}_2^2(\xi)}{8\tilde{n}_2^2(\xi)}, \tilde{\eta}_2(\xi) = \frac{\tilde{n}_5(\xi)\tilde{n}_1(\xi) - \tilde{n}_3^2(\xi)}{8\tilde{n}_3^2(\xi)}, \\ \tilde{\eta}_{xy}(\xi) &= \frac{\tilde{n}_1(\xi)\tilde{n}_6(\xi) - \tilde{n}_2(\xi)\tilde{n}_3(\xi)}{4\tilde{n}_2(\xi)\tilde{n}_3(\xi)}. \end{aligned} \quad (9)$$

The smoothed anellipticity parameter $\tilde{\eta}_3$ can be obtained from equation (7) by

$$\tilde{\eta}_3 = \frac{(1 + 2\tilde{\eta}_1)(1 + 2\tilde{\eta}_2) - (1 + \tilde{\eta}_{xy})^2}{2(1 + \tilde{\eta}_{xy})^2}. \quad (10)$$

We show the smoothing for three effective velocities V_0 , V_{nmo1} , and V_{nmo2} in Fig. 9. From the plots, we can see that the smoothing curves are quite similar for these three effective velocities \tilde{V}_0 , \tilde{V}_{nmo1} , and \tilde{V}_{nmo2} . Smoothing for anellipticity parameters, including the effective parameter computed from equation (10), is illustrated in Fig. 10. One can see that the smoothing curves are very similar for parameters $\tilde{\eta}_1$, $\tilde{\eta}_2$, and $\tilde{\eta}_{xy}$ but slightly different for $\tilde{\eta}_3$.

PRESERVED TRAVEL-TIME SMOOTHING IN ORTHORHOMBIC MEDIA WITH AZIMUTH VARIATION BETWEEN THE LAYERS

In the case of the azimuthal variation between orthorhombic (ORT) layers, we have to apply the rotation operator in the X-Y plane by $(\begin{smallmatrix} \cos \phi & \sin \phi \\ -\sin \phi & \cos \phi \end{smallmatrix})$ to equation (6) to specify the clockwise rotation azimuth.

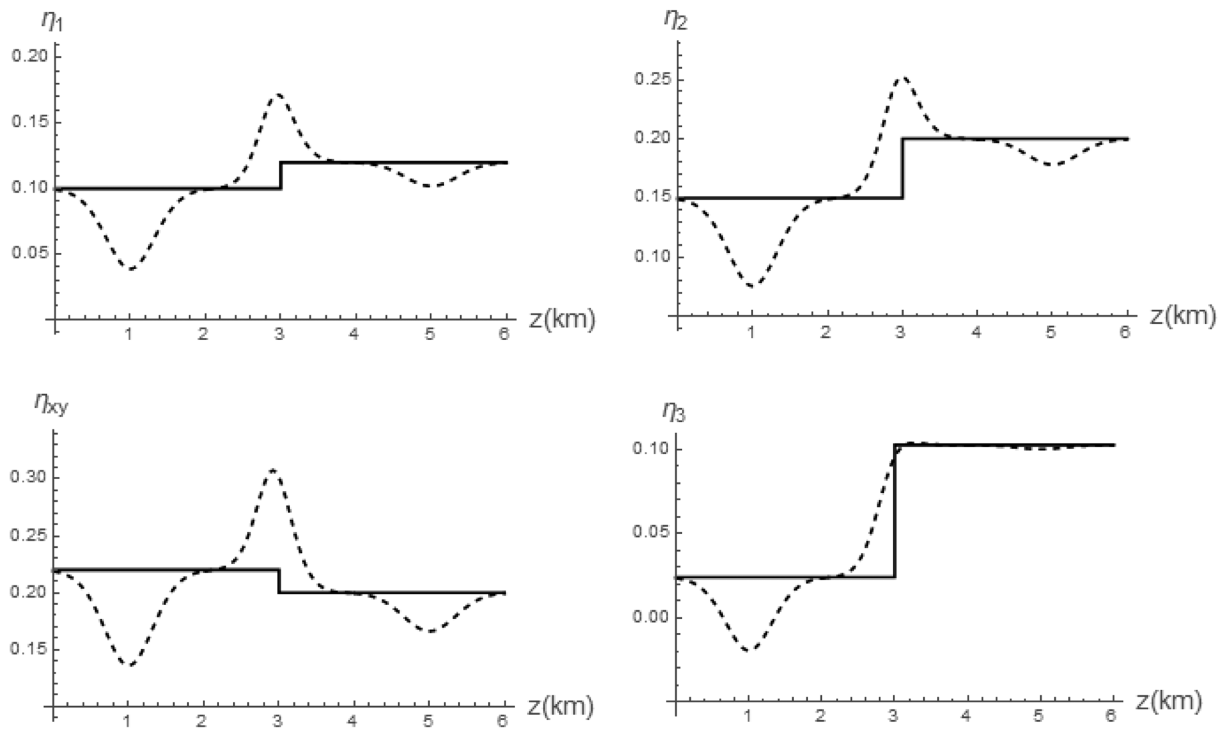


Figure 10 Four anellipticity parameters before and after smoothing for the ORT model. The unsmoothed and smoothed parameters are shown by solid and dashed lines, respectively.

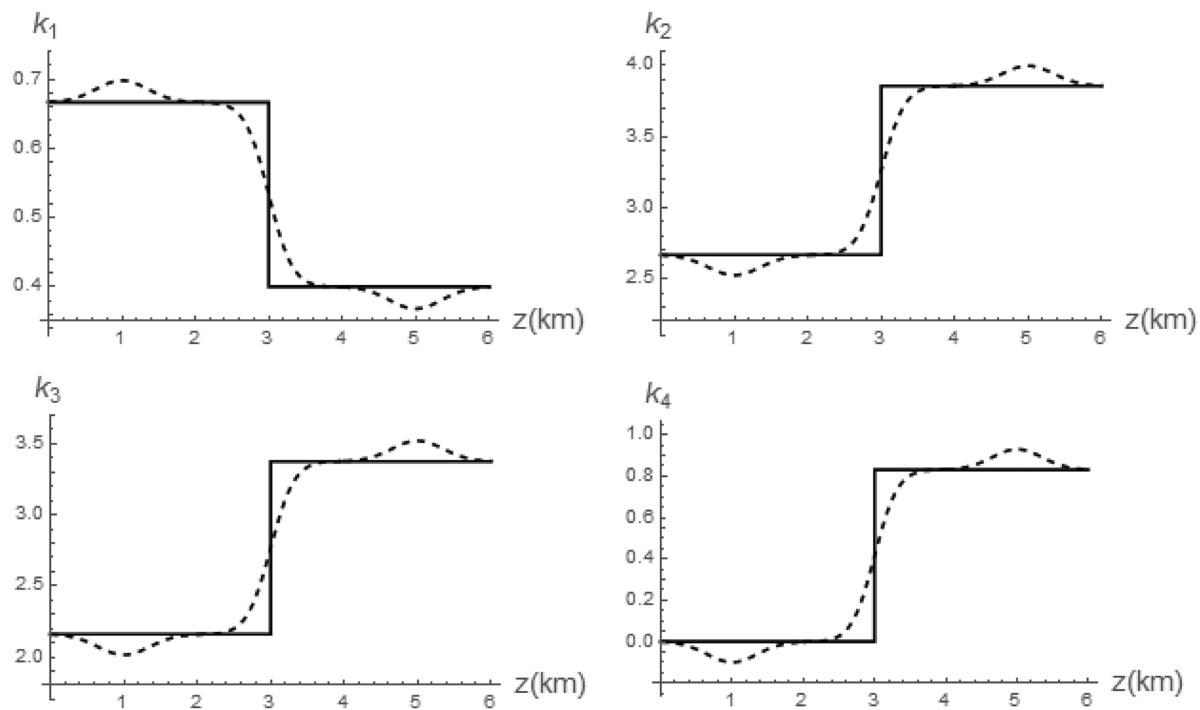


Figure 11 The composite parameters before and after smoothing for the ORT_ϕ model. The unsmoothed and smoothed parameters are shown by solid and dashed lines, respectively.

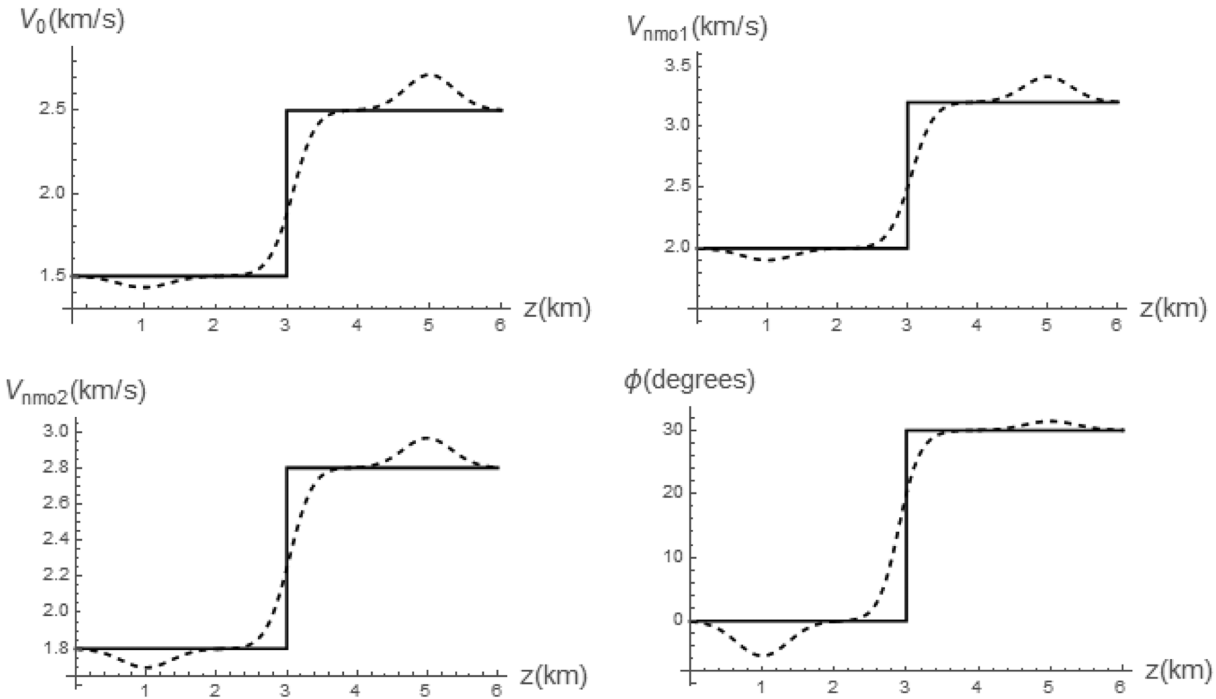


Figure 12 The effective velocities and effective azimuth before and after smoothing for the ORT_ϕ model. The unsmoothed and smoothed parameters are shown by solid and dashed lines, respectively.

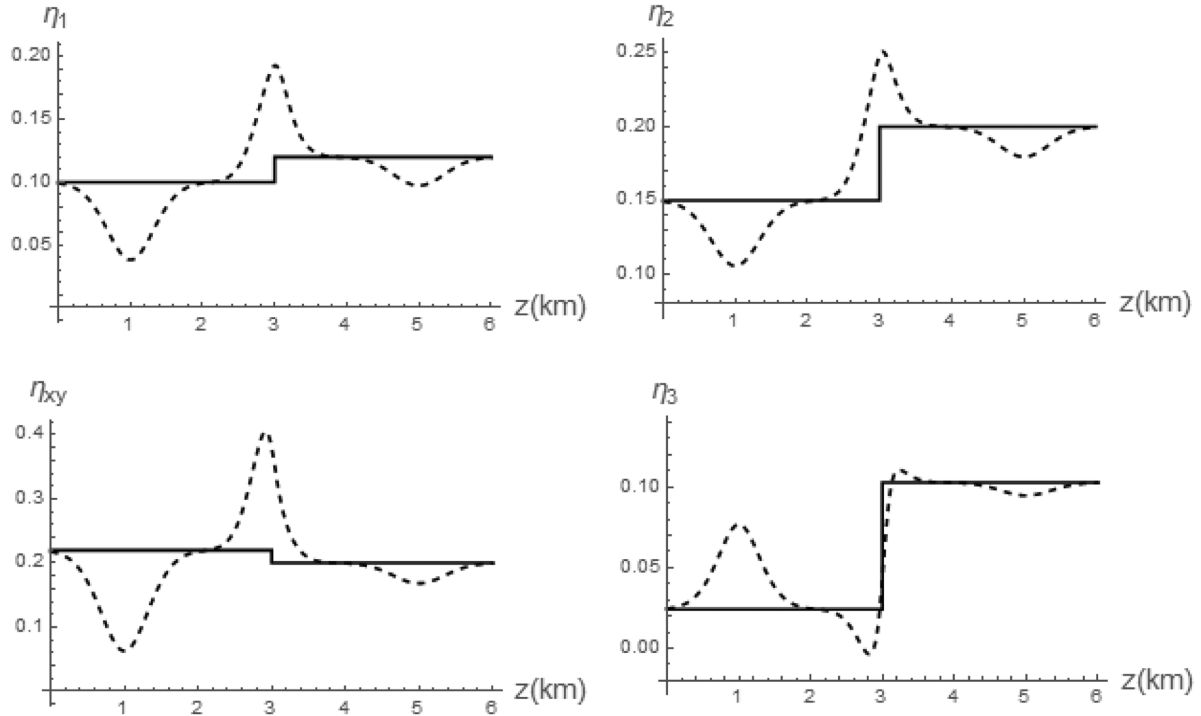


Figure 13 Four anellipticity parameters before and after smoothing for the ORT_ϕ model. The unsmoothed and smoothed parameters are shown by solid and dashed lines, respectively.

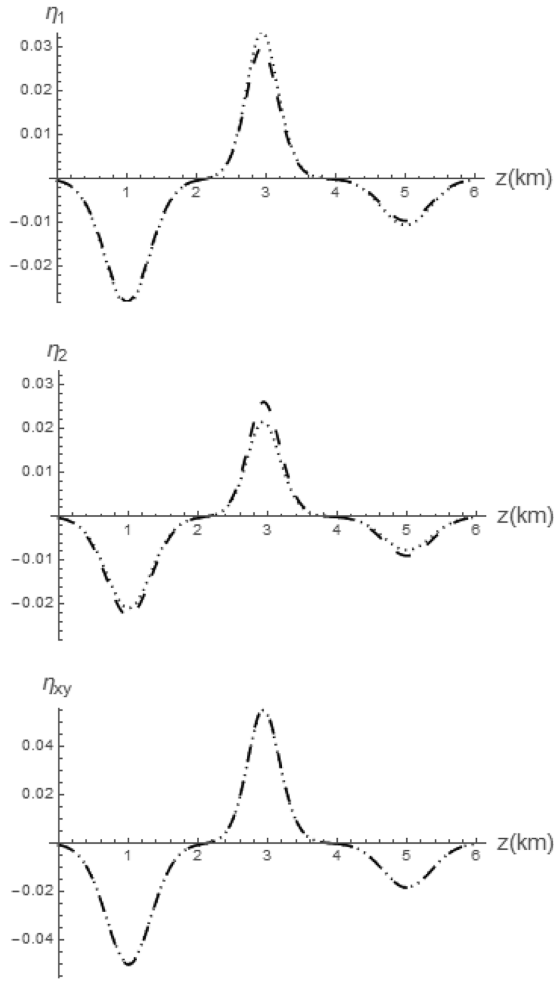


Figure 14 The PTS results in smoothing-induced anellipticity: (top) η_1 , (middle) η_2 , and (bottom) η_{xy} . The anellipticity from the ORT and ORT_ϕ models are shown in dashed and dotted lines, respectively.

The effective kinematic properties of the ORT model with the azimuth variation between layers can be found in Stovas (2015). The series for vertical slowness takes the form

$$\begin{aligned} q(p_x, p_y) = & \frac{1}{V_0} - \frac{1}{2V_0} \left(V_{nm01}^2 \cos^2 \phi + V_{nm02}^2 \sin^2 \phi \right) p_x^2 \\ & - \frac{1}{2V_0} \left(V_{nm01}^2 \sin^2 \phi + V_{nm02}^2 \cos^2 \phi \right) p_y^2 \\ & - \frac{1}{2V_0} \left(V_{nm01}^2 - V_{nm02}^2 \right) \sin 2\phi p_x p_y - \frac{1}{8V_0} \\ & \times \left[(1+8\eta_1) V_{nm01}^4 \cos^4 \phi + (1+8\eta_2) V_{nm02}^4 \sin^4 \phi \right. \\ & \left. + \frac{1}{2}(1+4\eta_{xy}) V_{nm01}^2 V_{nm02}^2 \sin^2 2\phi \right] p_x^4 \\ & - \frac{1}{4V_0} \left[(1+8\eta_1) V_{nm01}^4 \cos^2 \phi - (1+8\eta_2) V_{nm02}^4 \sin^2 \phi \right. \end{aligned}$$

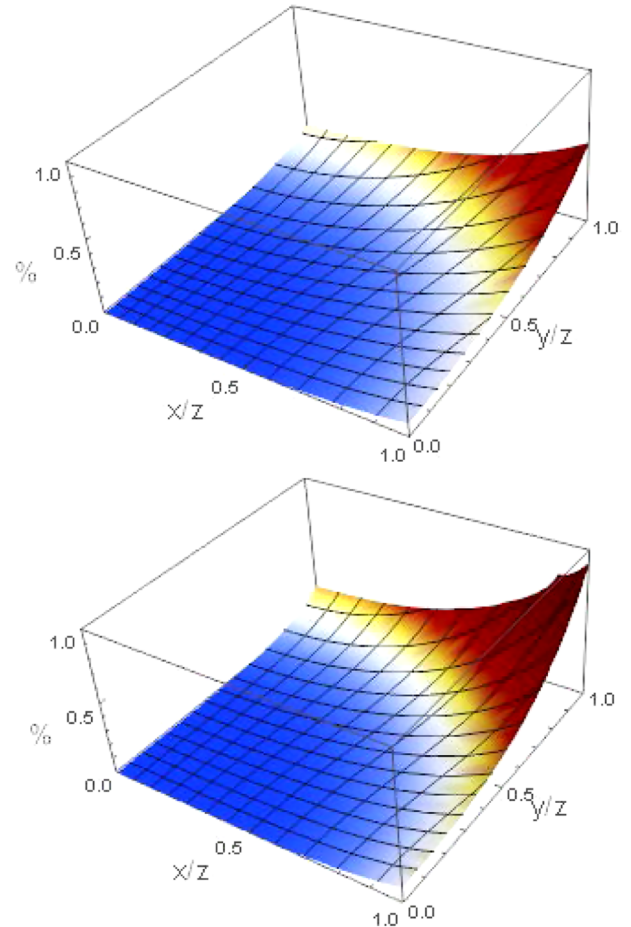


Figure 15 The travel-time error surface for (top) the ORT model and (bottom) the EI model.

$$\begin{aligned} & \left. - (1+4\eta_{xy}) V_{nm01}^2 V_{nm02}^2 \cos 2\phi \right] \sin 2\phi p_x^3 p_y \\ & - \frac{1}{16V_0} \left[3(1+8\eta_1) V_{nm01}^4 \sin^2 2\phi + 3(1+8\eta_2) \right. \\ & \times V_{nm02}^4 \sin^2 2\phi + (1+4\eta_{xy}) V_{nm01}^2 V_{nm02}^2 (1+3 \cos 4\phi) \left. \right] \\ & \times p_x^2 p_y^2 - \frac{1}{4V_0} \left[(1+8\eta_1) V_{nm01}^4 \sin^2 \phi - (1+8\eta_2) \right. \\ & \times V_{nm02}^4 \cos^2 \phi + (1+4\eta_{xy}) V_{nm01}^2 V_{nm02}^2 \cos 2\phi \left. \right] \\ & \times \sin 2\phi p_x p_y^3 - \frac{1}{8V_0} \left[(1+8\eta_1) V_{nm01}^4 \sin^4 \phi \right. \\ & + (1+8\eta_2) V_{nm02}^4 \cos^4 \phi + \frac{1}{2}(1+4\eta_{xy}) \\ & \left. \times V_{nm01}^2 V_{nm02}^2 \sin^2 2\phi \right] p_y^4 + \dots, \end{aligned} \quad (11)$$

where ϕ is specified as the azimuthal orientation of the vertical symmetry plane $[x, z]$ with respect to the global coordinate system.

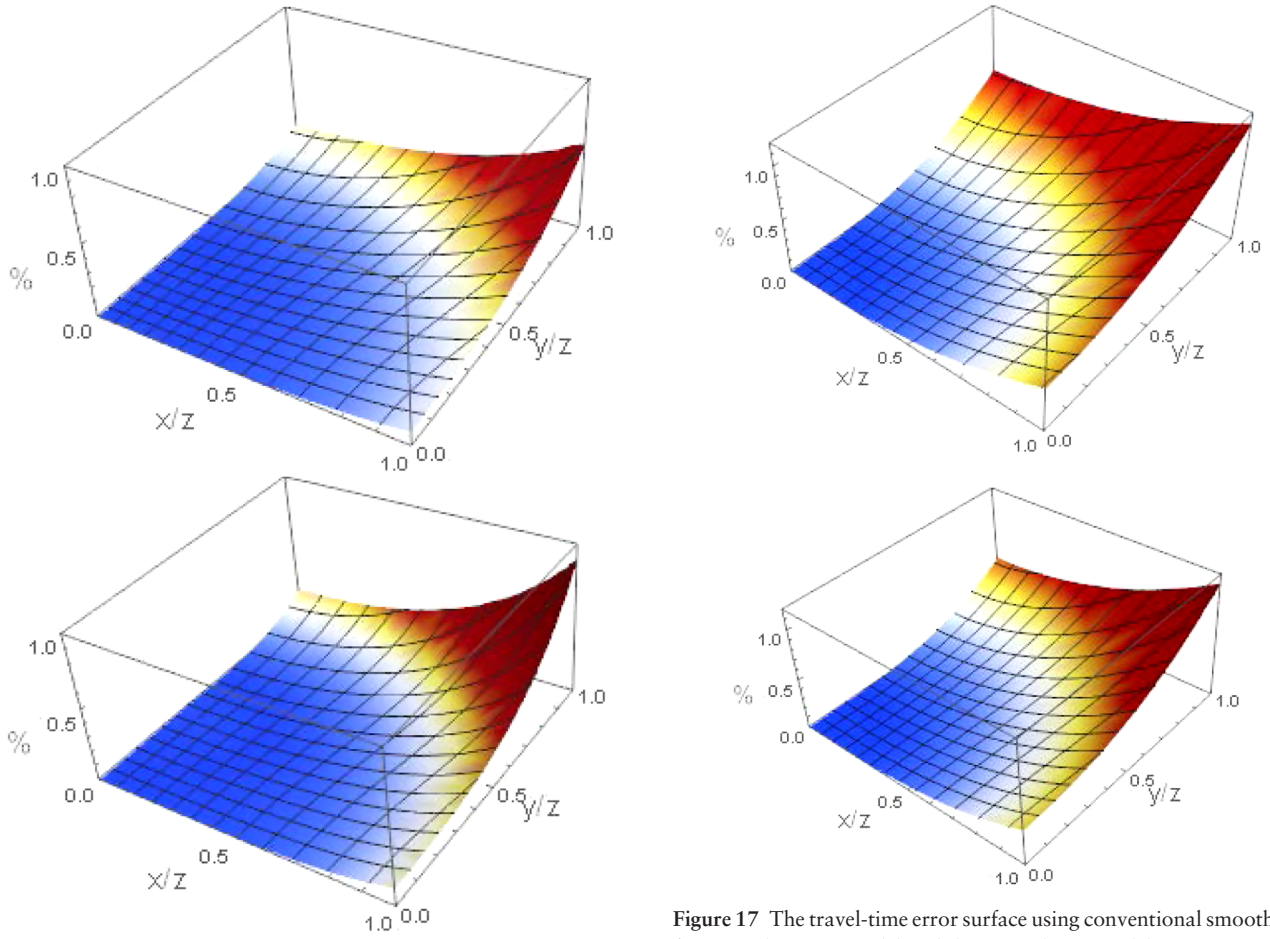


Figure 16 The travel-time error surface for (top) the ORT_ϕ model and (bottom) the EI_ϕ model.

In order to get the effective model parameters in this case, we smooth the composite parameters that are the series coefficients in equation (11). To convert the smoothed composite parameters into the models, we use two steps.

The equations for the first four composite parameters from equation (11) are

$$\begin{aligned} k_1 &= \frac{1}{V_0}, k_2 = \frac{1}{V_0} (V_{nmo1}^2 \cos^2 \phi + V_{nmo2}^2 \sin^2 \phi), \\ k_3 &= \frac{1}{V_0} (V_{nmo1}^2 \sin^2 \phi + V_{nmo2}^2 \cos^2 \phi), \\ k_4 &= \frac{1}{V_0} (V_{nmo1}^2 - V_{nmo2}^2) \sin 2\phi. \end{aligned} \quad (12)$$

These $k_j(j = 1..4)$ are smoothed into $\tilde{k}_j(j = 1, \dots, 4)$ and can be converted into three smoothed velocities and one

effective azimuth Φ by following equations:

$$\begin{aligned} \tilde{V}_0 &= \frac{1}{\tilde{k}_1}, \tilde{V}_{nmo1} = \sqrt{\frac{\tilde{k}_2 + \tilde{k}_3 + \sqrt{(\tilde{k}_2 - \tilde{k}_3)^2 + \tilde{k}_4^2}}{2\tilde{k}_1}}, \\ \tilde{V}_{nmo2} &= \sqrt{\frac{\tilde{k}_2 + \tilde{k}_3 - \sqrt{(\tilde{k}_2 - \tilde{k}_3)^2 + \tilde{k}_4^2}}{2\tilde{k}_1}}, \Phi \\ &= \frac{1}{2} \tan^{-1} \left(\frac{\tilde{k}_4}{\tilde{k}_2 - \tilde{k}_3} \right), \end{aligned} \quad (13)$$

where \tilde{V}_0 is the effective P-wave vertical velocity, and \tilde{V}_{nmo1} and \tilde{V}_{nmo2} are the effective normal moveout (NMO) velocities in symmetry planes. A similar technique is discussed by Grechka and Tsvankin (1999a, b). Φ stands for the effective azimuthal orientation.

To illustrate the first step, we define an azimuth-dependent ORT model ORT_ϕ by using the same two-layer ORT model as above with zero azimuth $\phi = 0^\circ$ in the upper

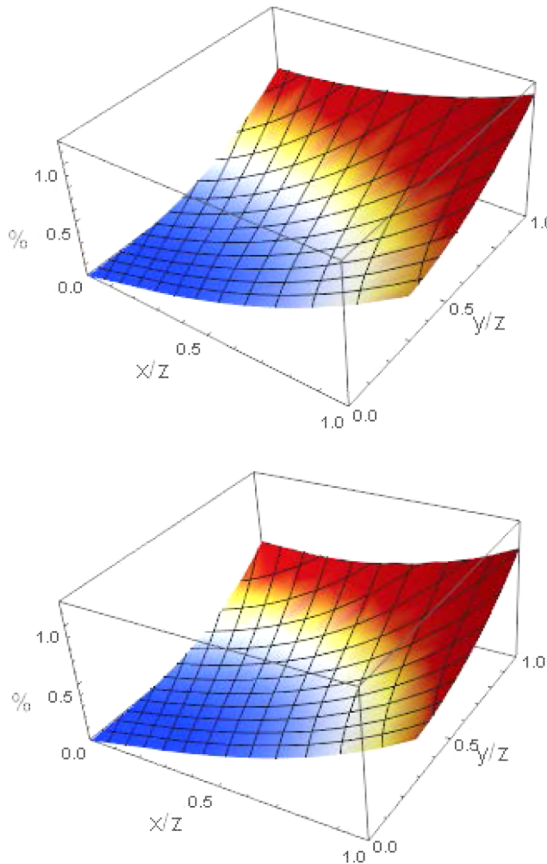


Figure 18 The travel-time error surface using conventional smoothing for (top) the ORT_ϕ model and (bottom) the EI_ϕ model.

layer and $\phi = 30^\circ$ in the lower layer. The composite parameters k_j ($j = 1, \dots, 4$) before and after smoothing are shown in Fig. 11. We can see that the curves are very similar with the ones before. The effective velocities \tilde{V}_0 , \tilde{V}_{nmo1} , and \tilde{V}_{nmo2} and azimuth Φ are shown in Fig. 12. From the comparison of Figs. 9 and 12, one can see that the presence of azimuth variation between the layers does not significantly affect the smoothed NMO velocities \tilde{V}_{nmo1} and \tilde{V}_{nmo2} . However, there is a difference in V_{nmo1} and V_{nmo2} between two cases of about 20 m/s with and without the azimuth variation between the layers. This difference for V_{nmo1} and V_{nmo2} has opposite sign.

In the second step, we solve the overdetermined system of the linear equations when estimating the effective anellipticity parameters. We apply the least squares method (Stovas 2015) to evaluate the effective parameters $\tilde{\eta}_1$, $\tilde{\eta}_2$, and $\tilde{\eta}_{xy}$. First, we define the effective anellipticity vector $\mathbf{N} = (\tilde{\eta}_1, \tilde{\eta}_2, \tilde{\eta}_{xy})^T$. The linear system of equations can be written in matrix form

$$\mathbf{UN} = \mathbf{DS}, \quad (14)$$

where the effective NMO slowness vector is defined as

$$\mathbf{S} = \left(\frac{1}{\tilde{V}_{nmo1}^4}, \frac{1}{\tilde{V}_{nmo2}^4}, \frac{1}{\tilde{V}_{nmo1}^2 \tilde{V}_{nmo2}^2} \right)^T, \quad (15)$$

and the azimuthal matrix $\mathbf{U}(\Phi)$ is given by

$$\mathbf{U} = \begin{pmatrix} 2\cos^4\Phi & 2\sin^4\Phi & 2\sin^2\Phi\cos^2\Phi \\ 2\sin 2\Phi\cos^2\Phi & -2\sin 2\Phi\sin^2\Phi & -\cos 2\Phi\sin 2\Phi \\ 6\sin^2 2\Phi & 6\sin^2 2\Phi & 1 + 3\cos 4\Phi \\ 2\sin 2\Phi\sin^2\Phi & -2\sin 2\Phi\cos^2\Phi & \cos 2\Phi\sin 2\Phi \\ 2\sin^4\Phi & 2\cos^4\Phi & 2\sin^2\Phi\cos^2\Phi \end{pmatrix}. \quad (16)$$

Note that the effective smoothed NMO velocities \tilde{V}_{nmo1} and \tilde{V}_{nmo2} and the effective azimuth Φ are precomputed in equation (13).

The least squares method gives the solution of equation (14) as follows:

$$\begin{aligned} \mathbf{N} &= \mathbf{GS}, \\ \mathbf{G} &= \mathbf{FD}, \\ \mathbf{F} &= (\mathbf{U}^T \mathbf{U})^{-1} \mathbf{U}^T, \end{aligned} \quad (17)$$

where \mathbf{F} is a 3×5 matrix and $\mathbf{D} = (d_{ij})$ is a 5×3 matrix. The elements of matrix \mathbf{D} are defined in the Appendix A.

If there is no azimuth variation between the layers ($\phi = 0^\circ$) or there is 90° azimuth variation ($\phi = \pi/2$), matrix \mathbf{F} has only three nonzero elements. The solution for effective anellipticity vector \mathbf{N} is reduced to the one defined in equation (9).

In order to smooth the parameters in this case, we need to define the matrix elements d_{ij} , ($i = 1, \dots, 5$; $j = 1, \dots, 3$) (see the Appendix A) and smooth each of these parameters by using the preserved travel-time smoothing (PTS) method described above. The effective velocities and effective azimuth are substituted from the computation in step one. The smoothed effective anellipticity parameters are computed from equation (17).

The effective anellipticity parameters in the ORT_ϕ model are shown in Fig. 13. Being compared with the results from the ORT model, the smoothing curves for parameters $\tilde{\eta}_1$, $\tilde{\eta}_2$, and $\tilde{\eta}_{xy}$ in the ORT_ϕ model are similar but with different amplitudes, larger for $\tilde{\eta}_1$ and $\tilde{\eta}_{xy}$, but smaller for $\tilde{\eta}_2$. The smoothed parameter $\tilde{\eta}_3$ is very different for the ORT and ORT_ϕ models.

Note that the application of the PTS method in the ORT and ORT_ϕ models results in smoothing-induced anellipticity. We illustrate this by using two models with ($\eta_1 = \eta_2 = \eta_{xy} = 0$), without (EI), and with (EI_ϕ) azimuth variations. The

smoothing-induced anelliptic parameters for the EI and EI_ϕ models are shown in Fig. 14. We can see that the magnitude anelliptic parameters η_1 and η_2 are different for these models, whereas parameter η_{xy} is very similar. The biggest anomaly for smoothing-induced anelliptic parameters is always located at the interface depth.

THE ACCURACY IN TRAVEL-TIME

To illustrate the accuracy by the preserved travel-time smoothing (PTS) method for the orthorhombic (ORT) model, we use the parametric offset-travel time equations (Stovas 2015)

$$\begin{aligned} X(p_x, p_y) &= p_x \int_0^z \frac{V_{nmo1}^2}{f_1^{1/2} f_2^{3/2} V_0} F_2 d\xi, \\ Y(p_x, p_y) &= p_y \int_0^z \frac{V_{nmo2}^2}{f_1^{1/2} f_2^{3/2} V_0} F_1 d\xi, \\ T(p_x, p_y) &= \int_0^z \frac{F_1 p_y^2 V_{nmo2}^2 + F_2 p_x^2 V_{nmo1}^2 + f_1 f_2}{f_1^{1/2} f_2^{3/2} V_0} d\xi, \end{aligned} \quad (18)$$

where X and Y are the corresponding offset projections, and

$$\begin{aligned} F_1(\xi) &= (p_x^2 V_{nmo1}^2(\xi)(2\eta_1(\xi) - \eta_{xy}(\xi)) - 1)^2, \\ F_2(\xi) &= (p_y^2 V_{nmo2}^2(\xi)(2\eta_2(\xi) - \eta_{xy}(\xi)) - 1)^2, \\ f_1(\xi) &= 1 - (1 + 2\eta_1(\xi))p_x^2 V_{nmo1}^2(\xi) - (1 + 2\eta_2(\xi))p_y^2 V_{nmo2}^2(\xi) \\ &\quad + ((1 + 2\eta_1(\xi))(1 + 2\eta_2(\xi)) - (1 + \eta_{xy}(\xi))^2)p_x^2 p_y^2 \\ &\quad \times V_{nmo1}^2(\xi) V_{nmo2}^2(\xi), \\ f_2(\xi) &= 1 - 2\eta_1(\xi)p_x^2 V_{nmo1}^2(\xi) \\ &\quad - 2\eta_2(\xi)p_y^2 V_{nmo2}^2(\xi) + (4\eta_1(\xi)\eta_2(\xi) \\ &\quad - \eta_{xy}^2(\xi))p_x^2 p_y^2 V_{nmo1}^2(\xi) V_{nmo2}^2(\xi). \end{aligned} \quad (19)$$

We compute the relative travel-time error due to smoothing for the ORT and elliptic isotropic (EI) (Fig. 15) and the ORT_ϕ and EI_ϕ (Fig. 16) models. From the comparison of the error plots, one can see that the errors for the ORT_ϕ and EI_ϕ models are similar with the ones for the ORT and EI models. The travel-time error for the EI model is larger than the error for the ORT model, and the error for the EI_ϕ model is also larger than the one for the ORT_ϕ model. For all the models, the maximal travel-time error is very small.

In order to make a comparison, we also plot the travel-time errors by using conventional smoothing for the ORT and EI (Fig. 17) models and the ORT_ϕ and EI_ϕ (Fig. 18) models. Different from PTS, the model parameters ($1/V_0$, δ_1 , δ_2 , ε_1 ,

ε_2 , and δ_3) are smoothed directly in conventional smoothing using the same smoothing operator in equation (3); δ_i and ε_i ($i = 1, 2$) are the Thomsen parameters in the corresponding symmetry planes. δ_3 is the anisotropy parameter defined by Vasconcelos and Tsvankin (2006)

$$\delta_3 = \frac{\varepsilon_2 - \varepsilon_1 - \eta_3 - 2\varepsilon_1\eta_3}{(1 + 2\varepsilon_1)(1 + 2\eta_3)}. \quad (20)$$

Compared with the errors in PTS, conventional smoothing results in larger error for long offset for all these four models.

CONCLUSIONS

We have developed the preserved travel-time smoothing (PTS) method for an orthorhombic (ORT) velocity model without and with azimuthal variation between the layers. Smoothing is performed for composite parameters that are different for the ORT and ORT_ϕ models. In computation of the anelliptic parameters for the ORT_ϕ model, the least squares method is used. We show that PTS results in smoothing-induced anellipticity and illustrate this for the EI and EI_ϕ models. The travel-time errors due to smoothing are sufficiently small for all the models.

ACKNOWLEDGEMENTS

The authors would like to thank China Scholarship Council and ROSE project for the financial support.

REFERENCES

- Alkhalifah T. 1998. Acoustic approximations for processing in transversely isotropic media. *Geophysics* **63**, 623–631.
- Alkhalifah T. 2003. An acoustic wave equation for orthorhombic anisotropy. *Geophysics* **68**, 1169–1172.
- Baina R., Zamboni E. and Lambaré G. 2006. How to cope with smoothing effect in ray based PSDM. *68th EAGE Conference & Exhibition*, Extended Abstracts.
- Červený V. 2001. *Seismic Ray Theory*. Cambridge, UK: Cambridge University Press.
- Fomel S. and Stovas A. 2010. Generalized nonhyperbolic moveout approximation. *Geophysics* **75**, U9–U18.
- Gonzalez R. and Woods R. 2008. *Digital Image Processing*, 3rd edn. Prentice Hall.
- Grechka V. and Tsvankin I. 1999a. 3-D moveout velocity analysis and parameter estimation for orthorhombic media. *Geophysics* **64**, 820–837.
- Grechka V. and Tsvankin I. 1999b. 3-D moveout inversion in azimuthally anisotropic media with lateral velocity variation: theory and case study. *Geophysics* **64**, 1202–1218.

- Schoenberg M. and Helbig K. 1997. Orthorhombic media: modeling elastic wave behavior in a vertically fractured earth. *Geophysics* **62**, 1954–1974.
- Stovas A. 2008. Kinematically equivalent velocity distributions. *Geophysics* **73**, VE369–VE375.
- Stovas A. 2015. Azimuthally dependent kinematic properties of orthorhombic media. *Geophysics* **80**, C107–C122.
- Thomsen L. 1986. Weak elastic anisotropy. *Geophysics* **51**, 1954–1966.
- Tsvankin I. 1997. Anisotropic parameters and P-wave velocity for orthorhombic media. *Geophysics* **62**, 1292–1309.
- Tsvankin I. 2012. Seismic signatures and analysis of reflection data in anisotropic media: SEG.
- Vasconcelos I. and Tsvankin I. 2006. Non-hyperbolic moveout inversion of wide-azimuth P-wave data for orthorhombic media. *Geophysical Prospecting* **54**, 535–552.
- Vinje V., Iversen E., Åstebøl K. and Gjøystdal H. 1996. Estimation of multivalued arrivals in 3D models using wavefront construction, Part I. *Geophysical Prospecting* **44**, 819–842.
- Vinje V., Stovas A. and Reynaud D. 2012. Preserved-traveltime smoothing. *Geophysical Prospecting* **61**, 380–390.

APPENDIX A

In order to smooth the model parameters by the preserved travel-time smoothing (PTS) method, we need to define the elements of matrix \mathbf{D} , which represent the composite parameters for the ORT_ϕ model (Stovas 2015)

$$\begin{aligned} d_{11} &= \frac{1}{V_0(\xi)}(1 + 8\eta_1(\xi))V_{nmo1}^4(\xi)\cos^4\phi, \\ d_{12} &= \frac{1}{V_0(\xi)}(1 + 8\eta_2(\xi))V_{nmo2}^4(\xi)\sin^4\phi, \\ d_{13} &= \frac{1}{V_0(\xi)}(1 + 4\eta_{xy}(\xi))V_{nmo1}^2(\xi)V_{nmo2}^2(\xi)\sin^2\phi\cos^2\phi, \\ d_{21} &= \frac{1}{V_0(\xi)}(1 + 8\eta_1(\xi))V_{nmo1}^4(\xi)\cos^2\phi\sin 2\phi, \\ d_{22} &= \frac{1}{V_0(\xi)}(1 + 8\eta_2(\xi))V_{nmo2}^4(\xi)\sin^2\phi\sin 2\phi, \\ d_{23} &= \frac{1}{V_0(\xi)}(1 + 4\eta_{xy}(\xi))V_{nmo1}^2(\xi)V_{nmo2}^2(\xi)\cos 2\phi\sin 2\phi, \quad (\text{A1}) \\ d_{31} &= \frac{1}{V_0(\xi)}(1 + 8\eta_1(\xi))V_{nmo1}^4(\xi)\sin^2 2\phi, \\ d_{32} &= \frac{1}{V_0(\xi)}(1 + 8\eta_2(\xi))V_{nmo2}^4(\xi)\sin^2 2\phi, \\ d_{33} &= \frac{1}{V_0(\xi)}(1 + 4\eta_{xy}(\xi))V_{nmo1}^2(\xi)V_{nmo2}^2(\xi)(1 + 3\cos 4\phi), \\ d_{41} &= \frac{1}{V_0(\xi)}(1 + 8\eta_1(\xi))V_{nmo1}^4(\xi)\sin^2\phi\sin 2\phi, \\ d_{42} &= \frac{1}{V_0(\xi)}(1 + 8\eta_2(\xi))V_{nmo2}^4(\xi)\cos^2\phi\sin 2\phi, \end{aligned}$$

$$\begin{aligned} d_{43} &= \frac{1}{V_0(\xi)}(1 + 4\eta_{xy}(\xi))V_{nmo1}^2(\xi)V_{nmo2}^2(\xi)\cos 2\phi\sin 2\phi, \\ d_{51} &= \frac{1}{V_0(\xi)}(1 + 8\eta_1(\xi))V_{nmo1}^4(\xi)\sin^4\phi, \\ d_{52} &= \frac{1}{V_0(\xi)}(1 + 8\eta_2(\xi))V_{nmo2}^4(\xi)\cos^4\phi, \\ d_{53} &= \frac{1}{V_0(\xi)}(1 + 4\eta_{xy}(\xi))V_{nmo1}^2(\xi)V_{nmo2}^2(\xi)\sin^2\phi\cos^2\phi, \end{aligned}$$

where V_0 is the P-wave vertical velocity, and the normal moveout velocities V_{nmo1} and V_{nmo2} are defined in the $[x, z]$ and $[y, z]$ symmetry planes, respectively. The cross-term parameter η_{xy} is defined in equation (7). Azimuth angle ϕ is specified as the azimuthal orientation of the vertical symmetry plane $[x, z]$ with respect to the global coordinate system.

We smooth the composite parameters shown in equation (A1) and substitute the results into the elements of matrix \mathbf{D} as follows:

$$\begin{aligned} D_{11} &= \frac{1}{4}(\tilde{V}_0\tilde{d}_{11} - \tilde{V}_{nmo1}^4\cos^4\Phi), \\ D_{12} &= \frac{1}{4}(\tilde{V}_0\tilde{d}_{12} - \tilde{V}_{nmo2}^4\sin^4\Phi), \\ D_{13} &= \frac{1}{2}(\tilde{V}_0\tilde{d}_{13} - \tilde{V}_{nmo1}^2\tilde{V}_{nmo2}^2\sin^2\Phi\cos^2\Phi), \\ D_{21} &= \frac{1}{4}(\tilde{V}_0\tilde{d}_{21} - \tilde{V}_{nmo1}^4\cos^2\Phi\sin 2\Phi), \\ D_{22} &= \frac{1}{4}(-\tilde{V}_0\tilde{d}_{22} + \tilde{V}_{nmo2}^4\sin^2\Phi\sin 2\Phi), \\ D_{23} &= \frac{1}{4}(-\tilde{V}_0\tilde{d}_{23} + \tilde{V}_{nmo1}^2\tilde{V}_{nmo2}^2\cos 2\Phi\sin 2\Phi), \\ D_{31} &= \frac{3}{4}(\tilde{V}_0\tilde{d}_{31} - \tilde{V}_{nmo1}^4\sin^2 2\Phi), \\ D_{32} &= \frac{3}{4}(\tilde{V}_0\tilde{d}_{32} - \tilde{V}_{nmo2}^4\sin^2 2\Phi), \\ D_{33} &= \frac{1}{4}(\tilde{V}_0\tilde{d}_{33} - \tilde{V}_{nmo1}^2\tilde{V}_{nmo2}^2(1 + 3\cos 4\Phi)), \\ D_{41} &= \frac{1}{4}(\tilde{V}_0\tilde{d}_{41} - \tilde{V}_{nmo1}^4\sin^2\Phi\sin 2\Phi), \\ D_{42} &= \frac{1}{4}(-\tilde{V}_0\tilde{d}_{42} + \tilde{V}_{nmo2}^4\cos^2\Phi\sin 2\Phi), \\ D_{43} &= \frac{1}{4}(\tilde{V}_0\tilde{d}_{43} - \tilde{V}_{nmo1}^2\tilde{V}_{nmo2}^2\cos 2\Phi\sin 2\Phi), \\ D_{51} &= \frac{1}{4}(\tilde{V}_0\tilde{d}_{51} - \tilde{V}_{nmo1}^4\sin^4\Phi), \\ D_{52} &= \frac{1}{4}(\tilde{V}_0\tilde{d}_{52} - \tilde{V}_{nmo2}^4\cos^4\Phi), \\ D_{53} &= \frac{1}{2}(\tilde{V}_0\tilde{d}_{53} - \tilde{V}_{nmo1}^2\tilde{V}_{nmo2}^2\sin^2\Phi\cos^2\Phi), \end{aligned} \quad (\text{A2})$$

where the effective velocities \tilde{V}_0 , \tilde{V}_{nmo1} , and \tilde{V}_{nmo2} and the effective azimuth Φ are already computed in equation (13).